Babes-Bolyai University
Faculty of Physics

Summary of Doctoral Thesis

PHOTOSENSITIZER-LOADED POLYMER-GOLD NANOPARTICLE HYBRIDS FOR ENHANCEMENT OF PHOTODYNAMIC THERAPY AND MULTIMODAL CELL IMAGING

By
Timea SIMON

Scientific advisor
Prof. Dr. Simion AŞTILEAN

CLUJ-NAPOCA
2013

TABLE OF CONTENTS

Thesis outline 1

Part I: Introduction and Review of Related Literature 2
1 Introduction 2
2 Literature Overview 2
2.1 Nanoparticle based approaches for cancer diagnosis and treatment 2
2.1.1 Photodynamic therapy (PDT) 2
2.2 Gold nanoparticles in medicine and nanomedicine 4
2.2.1 Optical properties of gold nanoparticles 4
2.2.2 Dark field microscopy based on gold nanoparticles for cell imaging 4
2.2.3 Optical response and photodynamic activity of molecules in presence of plasmonic nanoparticles 5
2.3 Hybrid nanoparticles in biomedical applications 6
2.3.1 Gold nanoparticle-polymer hybrids 6

Part II: Research Results and Discussions 7
3 Gold-Pluronic Core-Shell Nanoparticles: Synthesis, Characterization and Biological Evaluation 7
3.1 Preparation and characterization gold-Pluronic core-shell nanoparticles 7
3.1.1 Preparation of gold-Pluronic core-shell nanoparticles 7
3.1.2 Spectroscopic and morphologic characterization 7
3.2 Biological evaluation of gold-Pluronic core-shell nanoparticles 8
3.2.1 Cytotoxicity of the gold-Pluronic core-shell nanoparticles 8
3.2.2 Dark field imaging of cancer cells 9
4 Methylene blue-loaded Pluronic-nanogold hybrids for imaging and cancer therapy 10
4.1 Preparation and characterization of MB loaded gold-Pluronic nanoparticles 10
4.1.1 Preparation and characterization of Au-PF127 10
4.1.2 Preparation and characterization of Au-F127-MB nanoparticles 11
4.2 Investigation of the robustness and activity of Au-PF127-MB in view of their transfer to biomedical applications 12
4.2.1 Spectroscopic assessment of entrapped MB in Au-PF127-MB 12
4.2.2 Investigation of the photodynamic activity of Au-PF127-MB 14
4.3 Dark field imaging and LED-activated photodynamic therapy of cancer cells using AU-PF127-MB nanoparticles 15
4.3.1 Study of the cellular uptake of Au-PF127-MB using dark field microspectroscopy 15
4.3.2 LED-induced photodynamic therapy on HTB 177 cancer cells treated with Au-PF127-MB nanoparticles 16
5 Multimodal Imaging of Living Cells Using Photoactive Nanoaggregates 18
5.1 Samples preparation 18
5.1.1 Preparation of the gold nanoparticle aggregates 18
5.1.2 Conjugation gold nanoparticle aggregates with methylene blue 18
5.2 Characterization of the gold nano-aggregates 18
5.2.1 Morphological and optical characterization 18
5.3 Characterization of the methylene blue conjugated gold nano-aggregates 19
5.3.1 UV-Vis characterization 19
5.3.2 Time resolved fluorescence measurements 20
5.3.3 Stability in high ionic strength conditions 20
5.4 Multimodal spectroscopic detection inside living cells 20
5.4.1 Assessment of nanoparticle uptake by bright field microscopy 20
5.4.2 Intracellular SERS detection 20
5.4.3 Fluorescence lifetime imaging of GNPA-MB labeled cells 21
6 Final conclusions 22
References 23
List of publications 25

THESIS OUTLINE

My thesis is structured into two main parts containing six chapters. ***Part I***, entitled ***Introduction and Review of Related Literature***, is composed of two chapters. **Chapter 1** gives a short introduction to my research domain, motivating the subject of the thesis. **Chapter 2** presents a short literature overview regarding the application of nanotechnology to medicine, the ever-growing field called *nanomedicine*.

Part II, entitled ***Research Results and Discussions,*** presents in the course of three chapters the results obtained during my PhD in the *Nanobiophotonics Center* of the *Interdisciplinary Research Institute in Bio-Nano-Sciences* from Babes-Bolyai University in collaboration with *Laboratoire interdisciplinaire de Physique* from Joseph Fourier University, Grenoble.

Chapter 3 presents the preparation and characterization of Pluronic-gold core-shell nanoparticles, followed by the evaluation of their biological applicability. We point out the importance of purifying steps during the preparation process, by investigating the cytotoxicity of the Pluronic-gold nanoparticles. Finally, we show that the Pluronic-gold core-shell nanoparticles can serve as contrast agents for dark field scattering imaging.

The first part of **Chapter 4** presents the fabrication and characterization of a new class of hybrid nanoparticles, whereas the second part investigates their pertinence in cancer cell imaging and therapy. Pluronic-gold nanohybrids were prepared in a single step using Pluronic F127 block co-polymer as both reducing and stabilizing agent, then the photodynamic agent, Methylene Blue (MB) was loaded into the nanohybrids. As the therapeutic performance of MB may alter in various environmental conditions, a special attention is dedicated to investigate its properties upon loading into the nanohybrids. Henceforward, we evaluate the uptake of the nanohybrids by HTB cancer cells using dark field scattering microscopy. Subsequently, we demonstrate that our nanohybrids can be explored in photodynamic therapy of cancer cells using a light emitting diode (LED) to activate the encapsulated photosensitizer.

In **Chapter 5** the preparation of some multimodal imaging agents based on small gold nanoparticle aggregates is presented. Charge destabilization of citrate capped gold nanospheres underlies the formation of the aggregates followed by subsequent stabilization with Pluronic block co-polymer, which further mediates the conjugation with the fluorescent label molecule, Methylene Blue. The functionality of the obtained gold nanoaggregate-methylene blue conjugates to serve as multifunctional intracellular contrast agents is highlighted. On the one hand, the ability of the nanoparticles to perform as effective spectroscopic nano-tags *in vitro* through Surface Enhanced Resonant Raman Scattering (SERRS) is proved. On the other hand, we demonstrate the nanoparticles pertinence in Fluorescence Lifetime Imaging (FLIM) of cancer cells.

The final conclusions and the future perspectives are summarized in **Chapter 6**.

Keywords: gold nanoparticles, Pluronic, methylene blue, dark field imaging, photodynamic therapy, SERS, FLIM

PART I: INTRODUCTION AND REVIEW OF RELATED LITERATURE

1 Introduction

Nanomedicine, defined as the application of nanotechnology to medicine, concerns the use of precisely engineered nano-sized material systems to develop novel therapeutic and diagnostic tools [1].

The main objective of this thesis is to design stable and biocompatible polymer-gold nanoparticle hybrids able to carry photosensitizing molecules. Our strategy to combine methylene blue with Pluronic-gold hybrid nanoparticles represents a valuable development in the field of multifunctional nanomaterials. The versatility of these types of nanoparticles consists in the multimodal spectroscopic detection and imaging capacity combined with the enhanced therapeutic effectiveness against cancer cells.

2 Literature Overview

2.1 Nanoparticle based approaches for cancer diagnosis and treatment

By developing precisely manufactured targeted nanoparticles, nanotechnology aims to revolutionize the treatment of cancer, offering promising strategies to selectively deliver high concentrations of cytotoxic agents or imaging labels directly to the cancer site.

To date, various types of drug delivery nanoplatforms have been designed to carry tumor-killing agents, such as chemotherapeutics, photosensitizing agents or to deliver genes and proteins. Due to their high loading capacity, polymeric nanoparticles [2] and liposomes [3] are more intensively used in drug delivery applications compared to other types of nanoparticles. In addition to drug delivery nanosystems, cancer nanotherapeutics also includes the local thermal treatment of cancer employing photothermal agents, such as noble metal nanoparticles or carbon based nanomaterials which induce temperature increase in the target zone upon irradiation.

2.1.1 Photodynamic therapy (PDT)

PDT was the first drug-device combination approved by the Food and Drug Administration (FDA) almost two decades ago. It denotes a two-step therapeutic technique by which a photosensitizer molecule is delivered to the targeted cells or tissues followed by its activation by irradiation with visible light [4].

2.1.1.1 Photophysical and photochemical processes involved in PDT

Upon irradiation with light of the appropriate wavelength, the photosensitizer becomes excited to the excited singlet state from which two possible routes exist: relaxing back to the ground state by emitting a fluorescent photon or to excited triplet states via intersystem crossing . From triplet excited states there are also two possible mechanisms to occur: the photosensitizer can relax back to the ground state by emitting a phosphorescent photon or transfer energy to another molecule via a radiationless transition. The quenching mechanism of the triplet state of the sensitizer can occur via type I or type II. The *type I* mechanism involves the interaction with the biological substrate to yield radicals and radical ions. *Type II* mechanism results from an energy transfer from the triplet state of the sensitizer to ground state molecular oxygen, leading to the generation of an excited state of oxygen known as singlet oxygen [5].

2.1.1.2 Photosensitizers

Photosensitizers used in PDT are commonly classified as first, second and third generations. Briefly, the first generation photosensitizers include hematoporphyrin derivative and Photofrin. The second generation photosensitizers have been developed since the late 1980s to overcome the disadvantages of the first generation photosensitizers. The third generation photosensitizers are referred to the second generation photosensitizer conjugates, which are coupled to or loaded in various carrier molecules or nanoparticles for selective accumulation and targeting within tumor tissue.

2.1.1.3 Nanoparticle formulations for photodynamic therapy

The approach of encapsulation into nanocarriers of the photosensitizers can take advantage of the enhance permeability and retention (EPR) effect to improve the cellular uptake and the relatively high loading capacity and themselves also can be endowed with targeting molecules to improve selective accumulation. The most frequently employed nanocarriers for photosensitizer delivery include polymeric micelles and liposomes.

2.1.1.4 Methylene Blue in photodynamic therapy

Methylene blue (MB) is a well known histological dye belonging to the phenothiazinium class of compounds [6]. MB exhibits a strong absorption band in the therapeutic window of the skin at 664 nm [7] and presents high quantum yield singlet oxygen generation. These characteristics coupled with the relatively low dark toxicity make MB proper candidate as photosensitizer for PDT. Despite of the large variety of disease treatable with MB, its clinical use has been hindered when systemically applied because it is usually reduced by enzymes to

leukomethylene blue (LMB), which is a colorless compound with negligible photodynamic activity. To overcome this drawback, several nanoformulations were recently proposed to carry and protect MB from enzymatic degradation [8,9,10].

2.2 Gold nanoparticles in medicine and nanomedicine

Due to their attractive characteristics, such as biocompatibility, distinctive optical properties and accessible preparation methods, a large variety of gold nanoparticles have been recently developed for imaging, diagnostic and therapeutic applications.

2.2.1 Optical properties of gold nanoparticles

In the case of nanoparticles with dimensions much smaller than the wavelength of the light, an incident electromagnetic field at a given frequency induces a resonant, coherent oscillation of the free electrons in the metal. The amplitude of the oscillation reaches maximum at a specific frequency, called *surface plasmon resonance* (SPR), which appears as a strong absorption band in the UV-visible spectrum [11].

In order to suit a specific application, the SPR of gold nanoparticles can be tuned over a wide spectral domain [12]. In the case of spherical nanoparticles by increasing in the nanosphere size, the SPR is red-shifted towards longer wavelength. However, the size tunability of the nanosphere SPR is limited to the visible region. Other methods to tune the SPR to the desired NIR wavelength include changing the shape of the nanoparticles to different anisotropic forms such as rod-shaped, nanotriangles, star-shaped nanoparticles, or aggregation of gold nanoparticles in well defined clusters.

2.2.2 Dark field microscopy based on gold nanoparticles for cell imaging

Dark-field microscopy represents one of the most popular bioimaging methods based on gold nanoparticles also employed in this thesis [13] When gold nanoparticles are excited by a broad white-light source, the light frequencies corresponding to the SPR are strongly scattered, which can be exclusively collected by using a specific microscopic configuration. Therefore, the nanoparticles are seen as bright spots with a color corresponding to the SPR frequency on a dark background. Gold nanoparticles with various shapes and sizes have been successfully employed in dark field microscopy applications, with the aim of detection of microbial cells, bioimaging of cancer cells, to reveal receptors on their surface, study of endocytosis or even to map out a tumor.

2.2.3 Optical response and photodynamic activity of molecules in presence of plasmonic nanoparticles

The enhanced electromagnetic field around the gold nanoparticles is known to have considerable effects on the organic molecules in their closed vicinity, giving rise to a number of remarkable phenomena with particular interest in imaging and detection applications.

2.2.3.1 Molecular fluorescence in presence of plasmonic nanoparticles

The interaction of the excited-state fluorophores with free electrons in the metal results in a change in the fluorescence emission level, i.e., quenching or enhancement. Quenching is due to the non-radiative energy transfer from the excited states of the fluorophores to the gold colloids, occurring typically at short distances from the metal surface (~ 0–5 nm). Within an optimal range of distances separating molecules from metal, the phenomena metal enhanced fluorescence (MEF) can be observed, typically result in increased intensities and decreased lifetimes [14].

2.2.3.2 Raman Scattering in presence of plasmonic nanoparticle (Surface Enhanced Raman Scattering)

Surface Enhanced Raman Scattering (SERS) relies on the significant enhancement of the Raman signal from Raman-active analyte molecules near nanostructured metallic surfaces [15]. The energy lost by the photon in the scattering process, termed as *Raman shift*, provides chemical and structural information about the molecule, in particular about their vibrational structure. SERS can provide amplification of the Raman signal up to 10^9 – 10^{11}, enabling even single molecule detection [16].

2.2.3.3 Photodynamic activity in presence of plasmonic nanoparticles

. The first observation of the positive influence of plasmonic structures on photodynamic processes was reported by Zhang et al. [17]. The observed Metal-Enhanced Singlet Oxygen Generation (MESOG) was attributed to the enhanced excitation rate due to the metal and the subsequent enhanced intersystem crossing and enhanced excited state triplet yield. Actually, there are two proposed mechanisms for the enhancement of the quantum yield of singlet oxygen production: (1) increase of the overall absorption efficiency (cross-section) of the photosensitizer by the nanoparticles or (2) energy transfer from the nanoparticle to the photosensitizer molecules. Consequently, the approach of conjugating photosensitizer molecules to noble metal nanoparticles may be of great significance for singlet oxygen based clinical therapy, such as PDT.

2.3 Hybrid nanoparticles in biomedical applications

Hybrid nanoparticles, combining more than one type of functional components offer the possibility for simultaneous cancer detection and therapy or even combination of different therapies which can considerably increase the effectiveness of the individual treatments. These types of nanomaterials are also referred as *theranostic agents*.

2.3.1 Gold nanoparticle-polymer hybrids

To date, many types of polymers have been exploited to fabricate gold nanoparticle-polymer hybrids with various morphologies, such as spherical core-shell structure, particle assemblies embedded in a polymer matrix or polymeric micelles decorated with small gold particles [18]. The preparation techniques can be divided into two major groups: (1) covalent linkage, the polymer molecules being immobilized on the gold atoms via gold-sulfur bonds and (2) physical adsorption which includes hydrophobic association and electrostatic interaction. Besides acting as drug carrier, interfacing of gold nanoparticles with polymers offers increased stability in biological environment and significantly improves their biocompatibility and they also permit the functionalization with targeting molecules for specific recognition of tumors.

2.3.1.1 Pluronic block co-polymers

Pluronic is a class of block copolymers registered as a trademark of BASF Corporation. These block copolymers consist of hydrophilic poly(ethylene oxide) (PEO) and hydrophobic poly(propylene oxide) (PPO) blocks arranged in PEO-PPO-PEO structure. Pluronic copolymers self-assemble into micelles, the core of the micelle being composed of hydrophobic PPO chains, while hydrophilic PEO chains form the corona of the micelle. The core of the micelles can be used for incorporation of various therapeutic or diagnostic reagents especially of hydrophobic drugs which can be hardly directly administrated because of their water-insolubility [19]. Another appealing characteristic of the class of Pluronic block copolymers is their high biocompatibility, the capability to sensitize multidrug resistant (MDR) cancer cells and passive drug targeting to tumors via the EPR effect.

.

PART II: RESEARCH RESULTS AND DISCUSSIONS

3 Gold-Pluronic Core-Shell Nanoparticles: Synthesis, Characterization and Biological Evaluation

3.1 Preparation and characterization gold-Pluronic core-shell nanoparticles

3.1.1 Preparation of gold-Pluronic core-shell nanoparticles

In the first step, gold nanoparticles were synthesized in organic medium using oleylamine as both reducing and stabilizing agent. Then, we transferred the oleylamine capped-nanoparticles to aqueous phase using Pluronic F127 copolymer. Pluronic anchors onto the surface of gold nanoparticles via hydrophobic interaction between oleylamine and the PPO segment of Pluronic, while hydrophilicity of the PEO chains ensures the water-solubility of the nanoparticles.

3.1.2 Spectroscopic and morphologic characterization

Optical absorption spectra of the obtained nanoparticles before and after the Pluronic coating are shown in **Figure 3-1**. Oleylamine capped nanoparticles dispersed in hexane show surface plasmon resonance at 518 nm, characteristic for individual spherical nanoparticles (spectrum a). The 5 nm red-shift in the plasmon band maximum after the phase-transfer (spectrum b) is due to the modification of the refractive index of the surrounding medium, demonstrating the adsorption of Pluronic onto the gold nanoparticles surface.

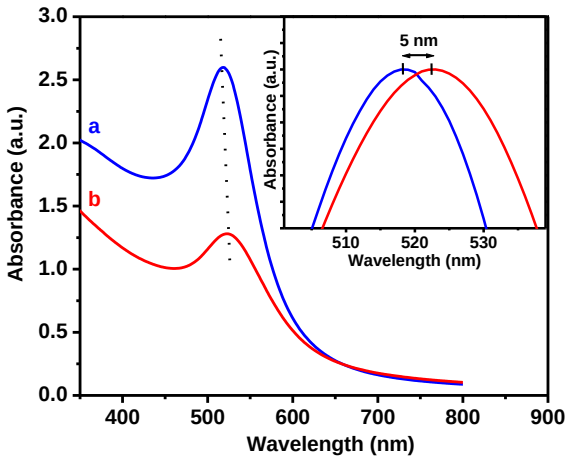

Figure 3-1 Absorption spectra of gold nanoparticles (a) and gold-Pluronic nanoparticles (b). The inset shows a magnified image of the normalized absorption maxima.

A characteristic TEM image of the nanoparticles is presented in **Figure 3-2 A**, revealing spherical, individual and uniform gold nanoparticles. Based on the histogram from **Figure 3-2 B**, the gold core of the obtained nanoparticles have a mean diameter of 9,4 nm with a standard deviation of 1,8 nm.

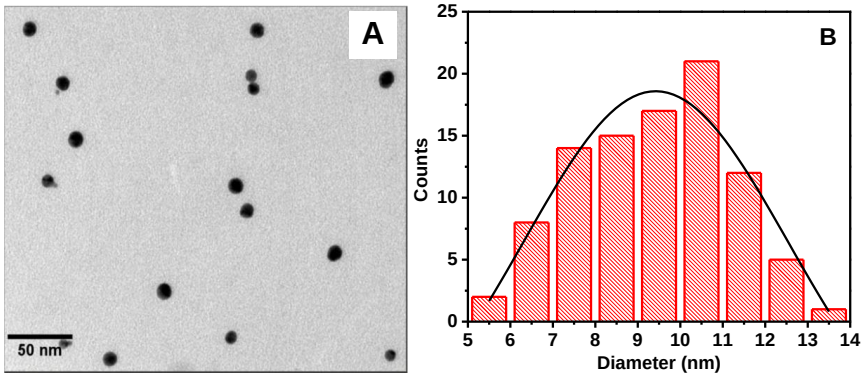

Figure 3-2 TEM image (A) and particle size distribution histogram of gold nanoparticles (B).

Conform to DLS measurements, oleylamine capped gold nanoparticles dispersed in hexane have an average hydrodynamic diameter of 13.48 nm. After the phase-transfer, the hydrodynamic diameter increased to 34.75 nm, the size difference indicating a polymer shell of ~ 10 nm, consistent with a single layer of Pluronic. The presence of the polymer shell on the gold nanoparticles surface is also demonstrated by the almost neutral Zeta-potential (4,48 mV) of the gold-Pluronic nanoparticles.

3.1.3 Stability in high ionic strength conditions

We investigated the stability of the gold-Pluronic nanoparticles in high molarity NaCl solution by monitoring the evolution of the UV-vis absorbance spectra over time. The obtained results indicate that the gold-Pluronic nanoparticles are highly stable in salted solution, the absorption spectra remaining almost unchanged even after incubation for 24 hours.

3.2 Biological evaluation of gold-Pluronic core-shell nanoparticles

3.2.1 Cytotoxicity of the gold-Pluronic core-shell nanoparticles

To estimate the toxicity of the gold-Pluronic nanoparticles, HTB 177 cells were incubated with different concentrations of purified and unpurified nanoparticles for different periods of time. The fate of the cells after incubation was assessed by fluorescence microscopy, using calcein-AM/PI double staining technique. **Figure 3-3** presents transmission and fluorescence images of HTB 177 cells incubated for 1 h with unpurified nanoparticles (0.5 nM) and for 24 h with purified nanoparticles (2 nM). Both transmission and fluorescence images indicate that

nanoparticles prepared by skipping the washing steps induced cell death even at low concentrations, while nanoparticles properly purified from the unbound oleylamine molecules and from any trace of hexane are highly biocompatible even after 24 hours incubation.

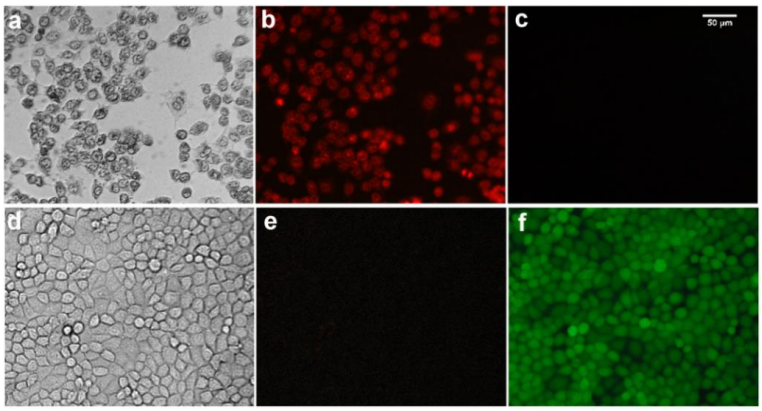

Figure 3-3 Transmission and fluorescence images of HTB cells incubated with unpurified (a,b and c) and purified (d, e and f) gold-Pluronic nanoparticles. Scale bar represents 50 µm.

3.2.2 Dark field imaging of cancer cells

Hereafter, the ability of gold-Pluronic nanoparticles to serve as scattering probes for cell imaging through dark field microscopy was investigated. **Figure 3-4** shows the dark field and corresponding transmission images of melanoma cells incubated with gold-Pluronic nanoparticles (1A, 2A) and with no nanoparticles (1B, 2B). The successful labeling of melanoma cells is clearly demonstrated by the yellowish-orange spots inside the cells incubated with nanoparticles, which are attributed to the well known scattering properties of gold nanoparticles.

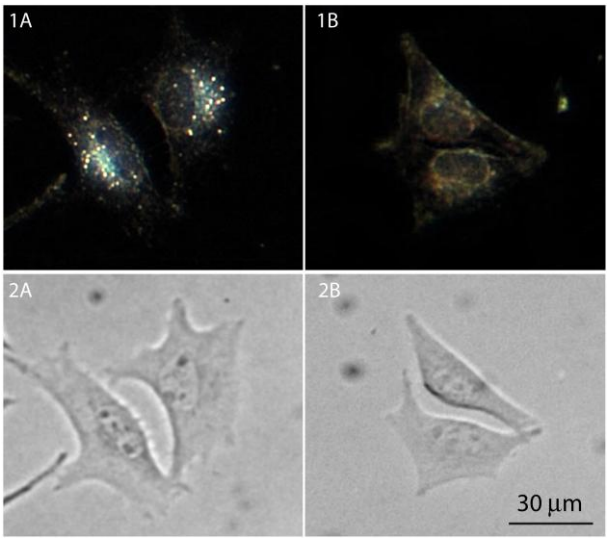

Figure 3-4 Dark field and corresponding transmission images of B16-F10 cells incubated with gold-Pluronic nanoparticles (1A, 2A) and control images without nanoparticles (1B, 2B).

4 Methylene blue-loaded Pluronic-nanogold hybrids for imaging and cancer therapy

4.1 Preparation and characterization of MB loaded gold-Pluronic nanoparticles

4.1.1 Preparation and characterization of Au-PF127

4.1.1.1 Synthesis of Pluronic nanogold hybrids

Gold nanoparticles were prepared by simply mixing an aqueous gold salt solution with with different concentrations of Pluronic F127 (0,5 mM, 1 mM, 2 mM, 5 mM and 10 mM), followed by the purification of the colloidal solution by centrifugation.

4.1.1.2 Spectroscopic and morphological characterization

Absorption spectra of the gold colloids obtained with various concentrations of Pluronic are illustrated in **Figure 4-1 A**. All spectra feature a common absorption band centered at about 540 nm which originates from localized surface plasmon resonance of individual gold nanoparticles in aqueous solution. Analysis of these spectra indicates that the polymer concentration of 2mM provides good stabilization of the gold nanoparticles with the minimal excess of polymer in the colloidal solution. The following experiments in this study were carried out using the sample of nanoparticles synthesized with 2 mM Pluronic F127 concentration.

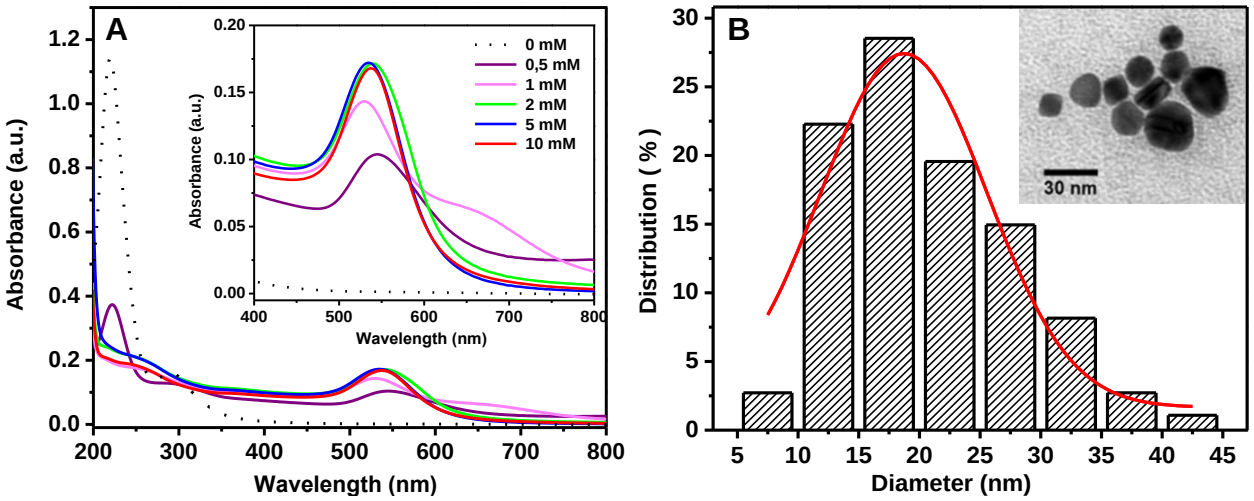

Figure 4-1 (A) Absorption spectra of as synthesized gold nanoparticles in aqueous solution, prepared with increasing concentrations of Pluronic F127. The inset shows magnified image of the plasmonic bands. The dotted line represents the absorption spectrum of $HAuCl_4 \cdot 3H_2O$ aqueous solution. (B) Particle size distribution histogram of Au-PF127 nanoparticles fitted with a Gaussian curve. The inset shows a TEM image of Au-PF127 nanoparticles.

The average diameter of the Au-PF127 nanoparticles was estimated to be 20±7 nm The corresponding histogram is presented in **Figure 4-1 B** fitted by a Gaussian curve, the inset showing a representative TEM image of the prepared nanoparticles. The DLS measurements indicate nanoparticles with a mean diameter of 41.5 nm including also the surface polymer, consistent with a single layer of Pluronic. Owing to the presence of polymer, the surface charge of the nanoparticles revealed by zeta potential measurements is almost neutral (-0.23 mV).

4.1.2 Preparation and characterization of Au-F127-MB nanoparticles

4.1.2.1 Tagging with MB

Tagging of Au-F127 with MB was realized by co-incubation at room temperature followed by purification from any unbound polymer and MB molecules by centrifugation.

4.1.2.2 Spectroscopic characterization

Loading of MB onto Au-PF127 was firstly characterized by UV-Vis absorption spectroscopy. The spectrum b in **Figure 4-2** shows the spectral features originating from the plasmonic resonances of gold nanoparticles and electronic absorption of MB molecules.

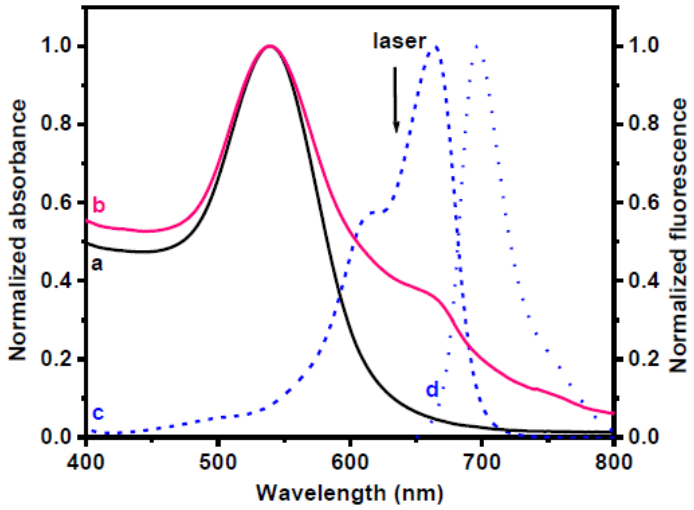

Figure 4-2 Normalized absorption spectra of Au-PF127 solution (a), Au-PF127-MB solution (b), MB solution (c) and normalized fluorescence spectrum of MB (d).

4.1.2.3 Stability of Au-F127-MB nanoparticles under biological conditions

The stability of the Au-PF127-MB nanoparticles in the presence of cell culture medium was confirmed by their almost unchanged spectroscopic signal after incubation for 24 h. It is noteworthy that no shift of the plasmonic absorption maximum occurs and the only effect is a slight broadening of the composite spectrum which can be related to the overlap with the light scattering of serum proteins from the cellular medium.

4.1.2.4 Leaching of MB in different ionic conditions

To quantify the possible desorption of MB from the Au-PF127-MB caused by the modification of the solvent polarity and ionicity around nanoparticles, the nanoparticles were incubated in different solutions (NaCl, ethanol, sodium dodecyl sulfate and cell culture medium), and the amount of MB released was estimated from the absorption spectra of the supernatant after centrifugation. The calculations indicate that 80 % from the initial amount of MB remains bound in the case of incubation in water, NaCl and cellular medium, 75% for that incubated in ethanol and 92% for the hybrids incubated with SDS solution. It is of high relevance in regard of biomedical applications, that the cellular medium does not promote extra leaching of MB.

4.2 Investigation of the robustness and activity of Au-PF127-MB in view of their transfer to biomedical applications

4.2.1 Spectroscopic assessment of entrapped MB in Au-PF127-MB

4.2.1.1 Dual fluorescence-SERS assessment

In this study, the SERS activity of Au-PF127-MB was investigated in order to gain information about the localization of MB regarding to the metallic surface. SERS spectra acquired from a drop of Au-PF127-MB colloidal solution reveal the fluorescence emission from MB, meanwhile the main characteristic Raman bands of MB can be easily identified (**Figure 4-3**, spectrum b). However, when measurements were repeated after the drop of colloid dried onto the glass substrate, the fluorescence signal was quenched while a strong, well-defined SERS spectrum of MB was readily detected (**Figure 4-2**, spectrum c). The results confirm the presence of MB molecules in two distinct states, either bound to the metal and providing SERS signal or isolated from the metal by polymeric spacer and generating fluorescence signal.

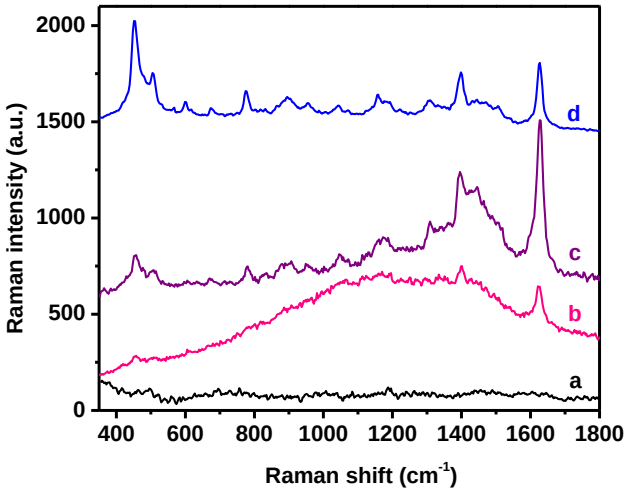

Figure 4-3 Raman spectrum of Au-PF127 (a), Dual SERS-fluorescence signal from Au-PF127-MB in aqueous solution (b), SERS from Au-PF127-MB in dried sample (c) and Raman spectrum of solid MB (d).

4.2.1.2 Study of the molecular form of the entrapped MB

The aggregation of photosensitizer upon encapsulation significantly alters their fluorescence and photodynamic properties; therefore we investigated the molecular form of MB upon loading to Au-PF127 by measuring the excitation spectra. The obtained result indicate that Au-PF127 nanoparticles preserve the monomeric form of MB molecules, offering significant benefits regarding their detection by fluorescence and their application as PDT agents.

4.2.1.3 Photophysics of the entrapped MB by time resolved fluorescence measurements

To elucidate the localization of MB in the Au-PF127 nanoparticles and to determine how the encapsulation affects its photophysical characteristics, we measured the fluorescence lifetime of the entrapped MB (see **Table 4-1**).

	τ_1 [ns]	A_1[%]	τ_2 [ns]	A_2[%]	χ^2
MB	0.4	100	-	-	1.039
PF127-MB	0.43	98	1.26	2	1.013
Au-PF127-MB	0.54	88	1.26	12	1.046

Table 4-1 Fluorescence decay parameters of MB, PF127-MB and Au-PF127-MB solutions. τ_1, τ_2 – fluorescence lifetimes; A_1, A_2 – percent distribution of the different components; χ^2statistical parameter indicating quality of the exponential fit.

The longer components can be attributed to the molecules residing in the hydrophobic domains of the Pluronic shell. Consequently, the shorter lifetime components are related to MB in hydrophilic environment, its increase being attributed to the increase of the local microviscosity

of the fluorophore. These favourable modifications in the photophysics of the MB encapsulated in the Au-PF127 nanoparticles represent a real advantage for the PDT-related applications.

4.2.2 Investigation of the photodynamic activity of Au-PF127-MB

4.2.2.1 Protection of MB against enzymatic reduction

In this section we proposed to verify if Pluronic can act as a protective shell against enzymes to prevent the degradation of MB. In our experiment we used baker's yeast as enzyme source and glucose as hydrogen-donor, whereas MB acted as hydrogen-acceptor. The decrease of the emission band of MB at 683 nm was monitored for 30 min at 40 °C under continuous magnetic (see **Figure 4-4**). The obtained results indicate that the Pluronic shell can protect the embedded photosensitizer against degradation by enzymes from biological medium, therefore Au-PF127-MB nanoparticles are suitable for biomedical applications.

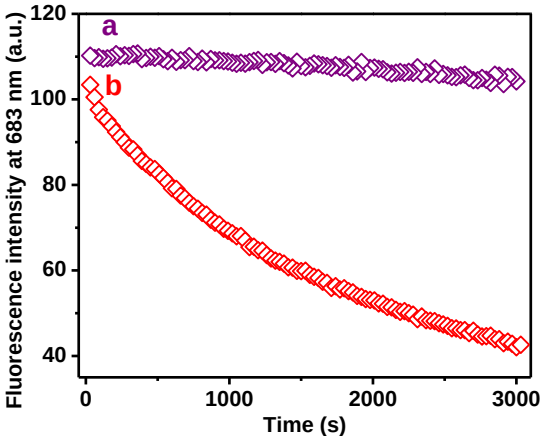

Figure 4-4 Time trace of fluorescence emission at 683 nm of Au-PF127-MB (a) and free MB (b) in the presence of yeast and glucose recorded at 40 °C.

4.2.2.2 Singlet oxygen generation measurements

In this part we investigate the potential of Au-PF127-MB nanohybrids in PDT, the ability of the adsorbed MB molecules to generate cytotoxic species. Herein, 1,3-Diphenylisobenzofuran (DPBF) was used to evaluate the release of singlet oxygen by the Au-PF127-MB nanohybrids in solution under resonant excitation of MB. DPBF reacts irreversibly with singlet oxygen, which causes a decrease in the intensity of the DPBF absorption band at 410 nm. **Figure 4-5** shows the time traces of the DPBF absorption decay as function of irradiation time together with the absorption spectra recorded before and after irradiation. The significant decrease in the absorption intensity of DPBF in the presence of the Au-PF127-MB relative to the reference

sample indicates the ability of the prepared hybrid nanoparticles to generate singlet oxygen, which is the main requirement for their future application in PDT.

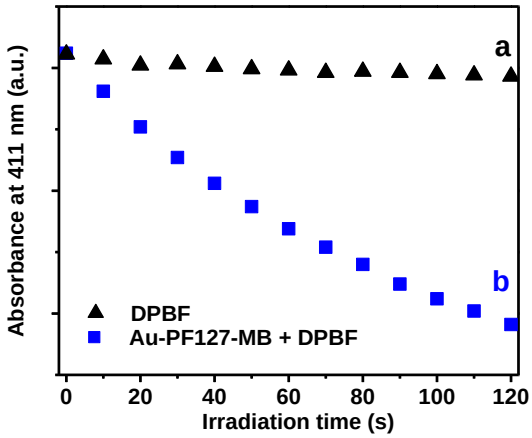

Figure 4-5 Time trace of absorption decay of the absorption intensity of DPBF at 410 nm in ethanol (a) and in the presence of Au-PF127-MB nanoparticles in ethanol (b).

4.3 Dark field imaging and LED-activated photodynamic therapy of cancer cells using AU-PF127-MB nanoparticles

4.3.1 Study of the cellular uptake of Au-PF127-MB using dark field microspectroscopy

Herein, we employed dark field microscopy to study the uptake and internalization of Au-PF127-MB nanoparticles by HTB 177 cells in function of the incubation periods.

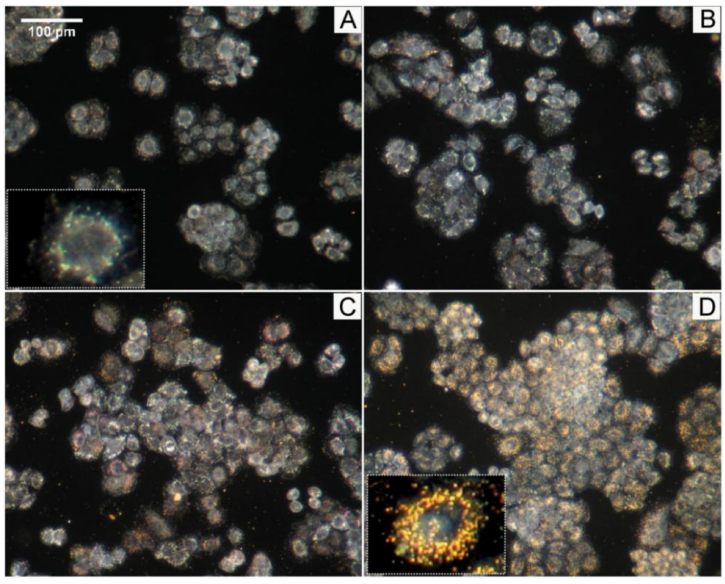

Figure 4-6 Dark field images of HTB 177 cells labeled with Au-PF127-MB for 0 h, 6 h, 15 h and 24 hours (A, B, C and D, respectively).

Figure 4-6 A presents a reference dark field image of HTB 177 cells without nanoparticles. Some bluish dots appear in the unlabeled cells due to the characteristic scattering of the intrinsic cellular organelles (inset **Figure 4-6 A**). After incubation for 6 hours (**Figure 4-6 B**), yellow-orange spots are observed inside a few number of cells, indicating a slight nanoparticle internalization. A more pronounced scattering also originating from Au-PF127-MB is observed after 15 h incubation (**Figure 4-6 C**), while 24 hours incubation results in a complete labeling of the cells (**Figure 4-6 D**).

The fact that the yellow to orange colored spots inside cells correspond to the surface plasmon enhancement of the scattered light by the internalized nanoparticles, was further confirmed by collecting the scattering spectra inside cells. **Figure 4-7** presents the magnified dark field images of the analyzed HTB 177 cells and the corresponding scattering spectra measured inside cells.

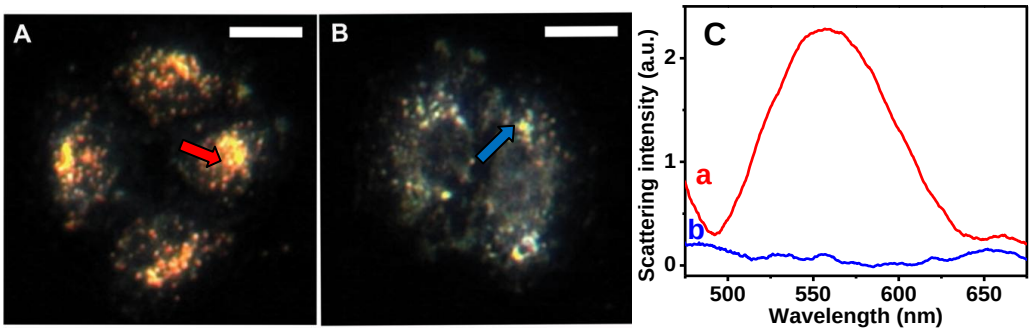

Figure 4-7 Dark field images of HTB 177 cells incubated with Au-PF127-MB for 24 h (A) and reference sample (B). Scale bar represents 20 μm. (C) Background corrected scattering spectra (a, b) measured inside cells from image A and B, respectively.

4.3.2 LED-induced photodynamic therapy on HTB 177 cancer cells treated with Au-PF127-MB nanoparticles

Besides protecting the photosensitizer from environmental factors and preserving its monomeric form, our strategy to encapsulate MB in the gold-Pluronic hybrids provides considerable advantages regarding the photodynamic activity of the nanoparticles by increasing the probability of singlet oxygen generation. Therefore, we can afford the use of a less invasive LED light source for irradiation, instead of high power output lasers. The Au-PF127-MB treated HTB 177 cells were irradiated at different light doses, controlled by modifying the light intensity and the irradiation time, respectively.

The state of the PDT subjected cells was evaluated 3 hours after the irradiation, using transmitted light and fluorescence microscopy. In transmitted light mode, modifications in the cellular morphology were followed, whereas for fluorescence assessment, the cells were double stained with calcein-AM and propidium iodide, which label viable and dead cells, respectively. The transmitted light and the merged fluorescence (calcein/IP) images of the Au-PF127-MB treated cells subjected to PDT at irradiation doses of 780 mW/cm^2, 640 mW/cm^2, 520 mW/cm^2 and 425 mW/cm^2 are presented in **Figure 4-8 a-d** and **A-D**, respectively. The cell viability after PDT was evaluated based on the fluorescence images using the Image J software. The results summarized reveal decreasing cell viability with the increase of the irradiation dose, descending down to 13 % viability at the highest irradiation dose (780 mW/cm^2).

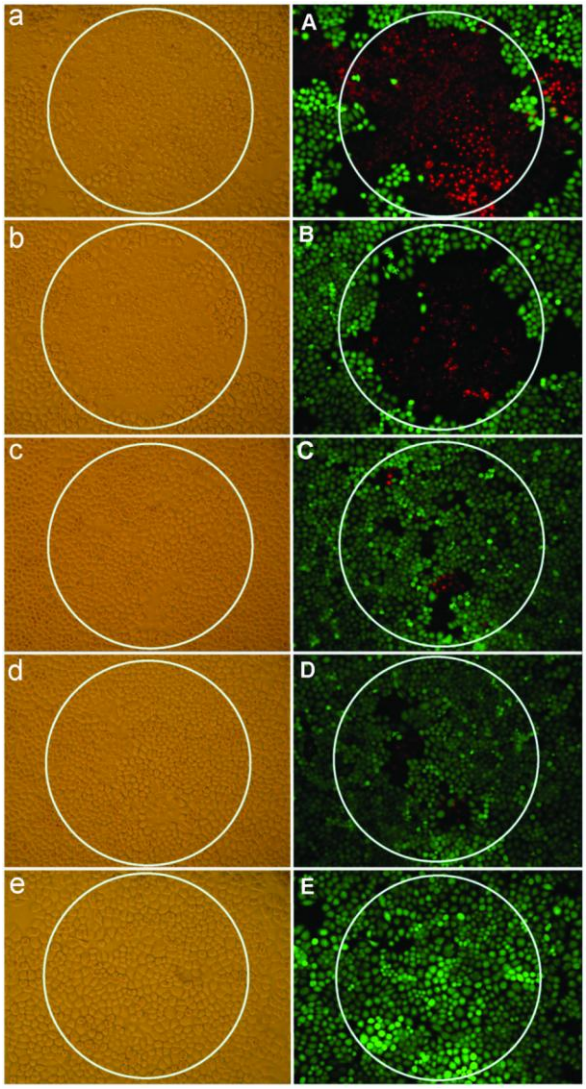

Figure 4-8 Transmitted light (a-d) and merged fluorescence (A-D) images of Au-PF127-MB incubated HTB 177 cells after with light doses of 780 mW/cm^2, 640 mW/cm^2, 520 mW/cm^2 and 425 mW/cm^2. The white circles represent the irradiated zones. Transmitted light (e) and merged fluorescence (E) images of Au-PF127 incubated HTB 177 cells after irradiation with the

5 Multimodal Imaging of Living Cells Using Photoactive Nanoaggregates

5.1 Samples preparation

5.1.1 Preparation of the gold nanoparticle aggregates

Citrate capped spherical gold nanoparticles with a mean diameter of 14±1 nm were synthesized by the aqueous reduction of $HAuCl_4$ with trisodium citrate according to the Turkevich-Frens method [21]. Aggregation of the nanoparticles was introduced by charge destabilization using NaCl in the presence of ethanol. The formed aggregates were stabilized with Pluronic F127 and purified by centrifugation.

5.1.2 Conjugation gold nanoparticle aggregates with methylene blue

Conjugation of GNPA with MB was realized by co-incubation at room temperature for 24 h, followed by their purification from unbound molecules by centrifugation and resuspension in ultrapure water.

5.2 Characterization of the gold nano-aggregates

5.2.1 Morphological and optical characterization

A representative TEM image of the formed nanoaggregates is presented in **Figure 5-1 A**, indicating a more pronounced chain-like organization in the case of larger cluster instead of a disordered aggregation. Bare majority of the nanoparticles (~ 32.5 %) remained individual, followed by an 18 % of dimers and 15 % of trimers, but we also found a number of larger aggregates (16 %) formed of more than 6 nanoparticles. The optical extinction spectra of the spherical nanoparticles (a) and GNPA (b) in solution are presented in **Figure 5-1 B**. Aggregation of the nanoparticles induces the broadening of the plasmonic band and the appearance of a secondary smaller band at longer wavelengths. The red-shift of 4 nm of the extinction maximum is consistent with an increase of the refractive index surrounding the nanoparticles, due to the absorption of the polymer at the nanoparticles surface. The attachment of the polymer at the nanoaggregates surface was further confirmed by Zeta-potential measurements. Citrate capped gold nanoparticles reveal a Zeta-potential of -44 mV which increased to -23 mV after the assembly and the subsequent stabilization with Pluronic.

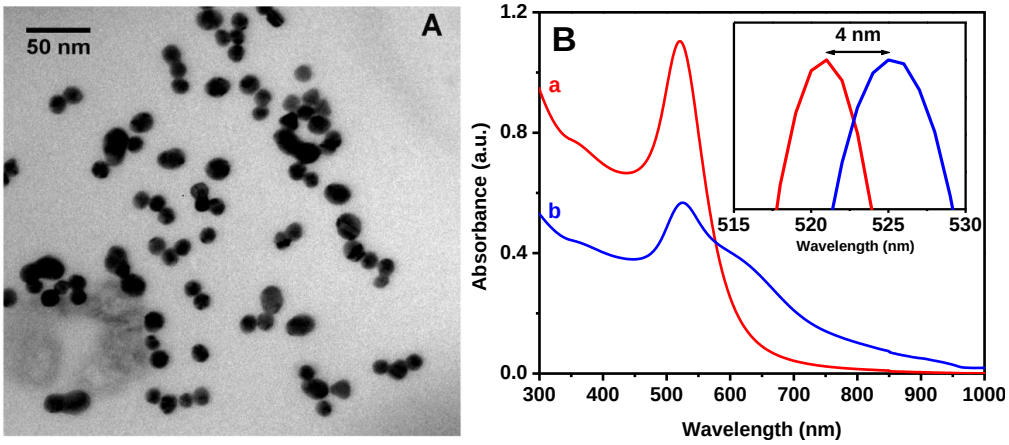

Figure 5-1 Representative TEM image of GNPA (A) and extinction spectra of gold nanoparticles (a) and GNPA (b) solutions (B).

5.3 Characterization of the methylene blue conjugated gold nano-aggregates

5.3.1 UV-Vis characterization

GNPA-MB reveal a spectroscopic feature of MB, manifesting in the increase of the intensity of the spectral band at the wavelength corresponding to the absorption of MB (**Figure 5-2**). The attachment of MB is also proven by a shift of 2 nm of the surface plasmon resonance band which can be assigned to the increase of the local refractive index surrounding the nanoaggregates.

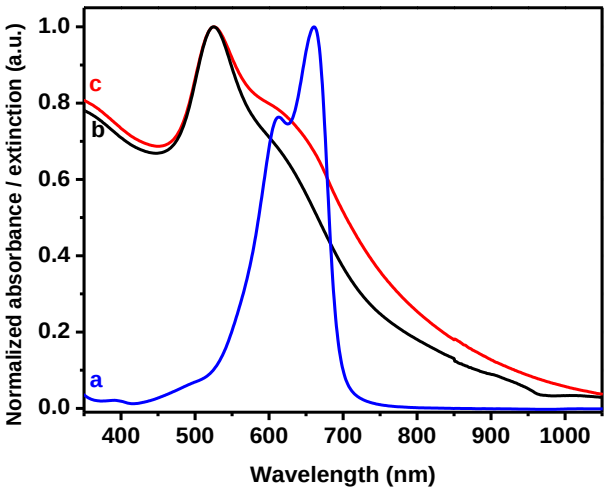

Figure 5-2 Normalized absorption spectrum of MB aqueous solution (a), normalized extinction spectrum of GNPA (b) and GNPA-MB nanotags (c).

5.3.2 Time resolved fluorescence measurements

As we have previously demonstrated in the case of Au-PF127-MB nanoparticles, interaction with Pluronic and gold nanoparticle can significantly alter the photophysical characteristics of MB. Similarly to those results, the appearance of a second larger component in the fluorescence lifetime of MB is also observed (1.27 ns) when conjugated to GNPA, as well as the lengthening of the shorter component (0.53 ns).

5.3.3 Stability in high ionic strength conditions

In order to simulate the behavior of the GNPA-MB nanoparticles in biological media, high molarity NaCl solution (at a final concentration of 200 mM) was added to the colloid and the optical extinction spectrum was monitored over time up to 24 h. GNPA-MB nanoparticles showed high stability in salted solution, the position and width of the plasmonic bands remaining almost unmodified.

5.4 Multimodal spectroscopic detection inside living cells

5.4.1 Assessment of nanoparticle uptake by bright field microscopy

Firstly, the uptake of GNPA-MB nanoparticles by cells was investigated by bright field transmission microscopy. Cells incubated with GNPA-MB for 24 h presented clearly visible black dots inside cells, spread along in the cytoplasmatic region, which can be clearly attributed to the presence of nanoparticles inside cells, most likely accumulated in the endosomes (**Figure 5-3**).

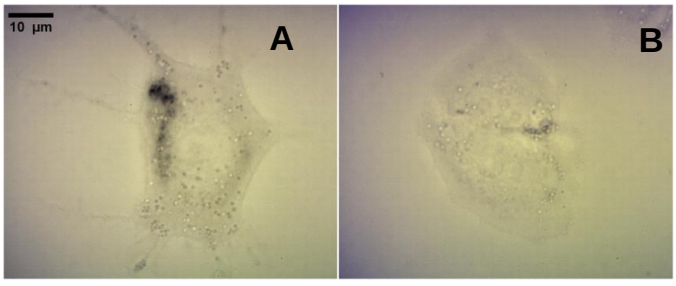

Figure 5-3 Transmission microscopy image of A549 cells incubated with GNPA-MB nanoparticles and without nanoparticles

5.4.2 Intracellular SERS detection

In order to investigate the intracellular SERS activity of our nanotags, human lung carcinoma cells were incubated with GNPA-MB naoparticles for 24 h. The 633 nm laser line used for excitation is resonant with the absorption band of MB, thus actually SERRS spectra

were measured during all the experiment. **Figure 5-4 B** presents the bright field reflection image of a GNPA-MB incubated cell, the bright spots representing the gold nanoparticles, known to strongly scatter the light relative to background scattering arising from cell components. Spectrum a from Figure 4.6 A represents a characteristic SERRS spectrum collected from the bright spot indicated by the arrow in **Figure 5-4 B**, which highly resembles to the spectrum collected from GNPA-MB solution (spectrum b). It is worth to mention that unlabeled cells show no specific fingerprint (spectrum d) and no cellular components were found to interfere with the Raman signature of MB in the spectrum collected from GNPA-MB incubated cells. This results is in good accordance with other literature reports, which demonstrate that Pluronic inhibits the adsorption of large molecules, such as proteins or lipids [22].

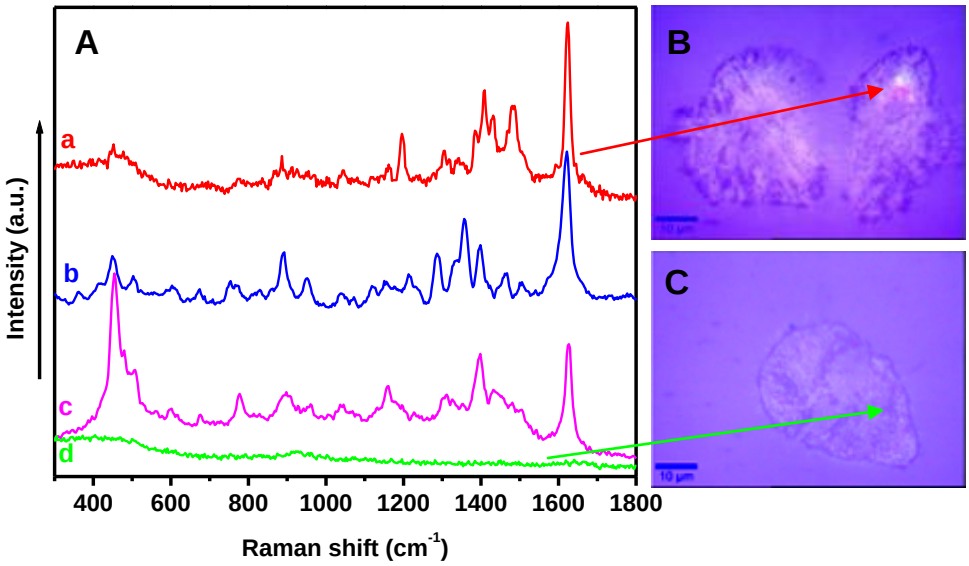

Figure 5-4 (A) SERRS spectrum of GNPA-MB nanotags inside cells (a), SERRS spectrum of GNPA-MB solution (b), ordinary Raman spectrum of MB (c) and background Raman scattering from control cells (d). (B) Bright-field reflection image of the GNPA-MB labeled A549 cells and (C) bright-field reflection image of control A549 cell.

5.4.3 Fluorescence lifetime imaging of GNPA-MB labeled cells

Figure 5-5 A shows the FLIM image of the control A549 cells without nanoparticles. A slight autofluorescence is emitted by the cells, with average lifetime of 2.5 ns. In the case of cell incubated with free MB, FLIM images revealed an accumulation the MB molecules in the lysosomes having a lifetime decreased to 0.27 ns (Figure 5-5 B). This lifetime shortening can be attributed to the aggregation of MB as a result of the high local concentration reached upon accumulation.

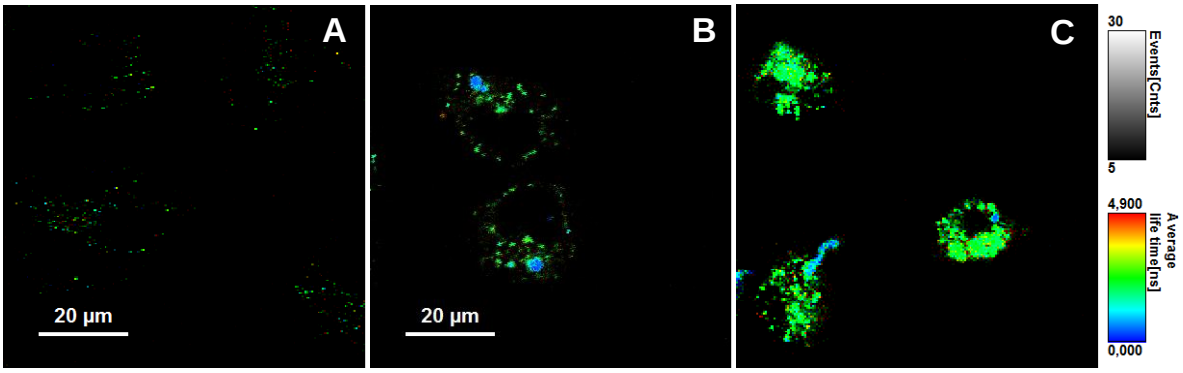

Figure 5-5 FLIM of A 549 cells (A), of MB labeled A 549 cells (B) and of GNPA-MB labeled A 549 cells (C)

The uptake of GNPA-MB by A549 cells has been confirmed by **Figure 5-5 C**, revealing a more uniform localization within the cytoplasmic region. A double exponential decay was observed in this case, with fluorescence lifetimes of 2.5 ns and 1.3 ns, arising from the autofluorescence of cell organelles and from GNPA-MB, respectively. However, a few dots similarly accumulated as free MB with appropriate lifetime value (0,25 ns), were found in the cells incubated with GNPA-MB. We ascribe this observation to a possible release of MB by GNPA-MB from the hydrophilic polymer corona as a consequence of interaction with biomolecules from cells.

6 Final conclusions

- We fabricated biocompatible and stable gold-Pluronic core-shell nanoparticles which can serve as contrast agents in dark field imaging of melanoma cells.
- We developed multifunctional methylene blue-loaded Pluronic-gold nanohybrids for cancer cell imaging and LED-activated photodynamic therapy.
- We fabricated methylene blue-conjugated gold nanoaggregates for multimodal cancer cell detection via FLIM and SERS.

REFERENCES

[1] Y.-C. Yeh, B. Creran, and V. M. Rotello, "Gold nanoparticles: preparation, properties, and applications in bionanotechnology," *Nanoscale*, vol. 4, no. 6, pp. 1871–1880, Mar. 2012.

[2] T. Gallavardin, M. Maurin, S. Marotte, T. Simon, A.-M. Gabudean, Y. Bretonnière, M. Lindgren, F. Lerouge, P. L. Baldeck, O. Stéphan, Y. Leverrier, J. Marvel, S. Parola, O. Maury, and C. Andraud, "Photodynamic therapy and two-photon bio-imaging applications of hydrophobic chromophores through amphiphilic polymer delivery," *Photochem. Photobiol. Sci.*, vol. 10, no. 7, pp. 1216–1225, Jun. 2011.

[3] T. M. Allen and P. R. Cullis, "Liposomal drug delivery systems: From concept to clinical applications," *Adv. Drug Deliv. Rev.*, vol. 65, no. 1, pp. 36–48, Jan. 2013.

[4] P. Agostinis, K. Berg, K. A. Cengel, T. H. Foster, A. W. Girotti, S. O. Gollnick, S. M. Hahn, M. R. Hamblin, A. Juzeniene, D. Kessel, M. Korbelik, J. Moan, P. Mroz, D. Nowis, J. Piette, B. C. Wilson, and J. Golab, "Photodynamic therapy of cancer: An update," *CA. Cancer J. Clin.*, vol. 61, no. 4, pp. 250–281, 2011.

[5] M. C. DeRosa and R. J. Crutchley, "Photosensitized singlet oxygen and its applications," *Coord. Chem. Rev.*, vol. 233–234, pp. 351–371, Nov. 2002.

[6] J. P. Tardivo, A. Del Giglio, D. Oliveira, C. Santos, D. S. Gabrielli, H. C. Junqueira, D. B. Tada, D. Severino, R. de Fátima Turchiello, and M. S. Baptista, "Methylene blue in photodynamic therapy: From basic mechanisms to clinical applications," *Photodiagnosis Photodyn. Ther.*, vol. 2, no. 3, pp. 175–191, Sep. 2005.

[7] H. C. Junqueira, D. Severino, L. G. Dias, M. S. Gugliotti, and M. S. Baptista, "Modulation of methylene blue photochemical properties based on adsorption at aqueous micelle interfaces," *Phys. Chem. Chem. Phys.*, vol. 4, no. 11, pp. 2320–2328, May 2002.

[8] W. Tang, H. Xu, E. J. Park, M. A. Philbert, and R. Kopelman, "Encapsulation of methylene blue in polyacrylamide nanoparticle platforms protects its photodynamic effectiveness," *Biochem. Biophys. Res. Commun.*, vol. 369, no. 2, pp. 579–583, May 2008.

[9] X. He, X. Wu, K. Wang, B. Shi, and L. Hai, "Methylene blue-encapsulated phosphonate-terminated silica nanoparticles for simultaneous in vivo imaging and photodynamic therapy," *Biomaterials*, vol. 30, no. 29, pp. 5601–5609, Oct. 2009.

[10] H. J. Hah, G. Kim, Y.-E. K. Lee, D. A. Orringer, O. Sagher, M. A. Philbert, and R. Kopelman, "Methylene blue-conjugated hydrogel nanoparticles and tumor-cell targeted photodynamic therapy," *Macromol. Biosci.*, vol. 11, no. 1, pp. 90–99, Jan. 2011.

[11] S. Link and M. A. El-Sayed, "Optical properties and ultrafast dynamics of metallic nanocrystals," *Annu. Rev. Phys. Chem.*, vol. 54, pp. 331–366, 2003.

[12] Y. Sun and Y. Xia, "Gold and silver nanoparticles: A class of chromophores with colors tunable in the range from 400 to 750 nm," *Analyst*, vol. 128, no. 6, pp. 686–691, Jan. 2003.

[13] A. Wax and K. Sokolov, "Molecular imaging and darkfield microspectroscopy of live cells using gold plasmonic nanoparticles," *Laser Photonics Rev.*, vol. 3, no. 1–2, pp. 146–158, 2009.

[14] K. Aslan, I. Gryczynski, J. Malicka, E. Matveeva, J. R. Lakowicz, and C. D. Geddes, "Metal-enhanced fluorescence: an emerging tool in biotechnology," *Curr. Opin. Biotechnol.*, vol. 16, no. 1, pp. 55–62, Feb. 2005.

[15] J. R. Lombardi and R. L. Birke, "A Unified View of Surface-Enhanced Raman Scattering," *Accounts Chem. Res.*, vol. 42, no. 6, pp. 734–742, Jun. 2009.

[16] Y. Wang and J. Irudayaraj, "Surface-enhanced Raman spectroscopy at single-molecule scale and its implications in biology," *Philos. Trans. R. Soc. B Biol. Sci.*, vol. 368, no. 1611, Feb. 2013.

[17] Y. Zhang, K. Aslan, M. J. R. Previte, and C. D. Geddes, "Metal-enhanced Singlet Oxygen Generation: A Consequence of Plasmon Enhanced Triplet Yields," *J. Fluoresc.*, vol. 17, no. 4, pp. 345–349, Jul. 2007.

[18] K. H. Bae, S. H. Choi, S. Y. Park, Y. Lee, and T. G. Park, "Thermosensitive Pluronic Micelles Stabilized by Shell Cross-Linking with Gold Nanoparticles," *Langmuir*, vol. 22, no. 14, pp. 6380–6384, Jul. 2006.

[19] M. Y. Kozlov, N. S. Melik-Nubarov, E. V. Batrakova, and A. V. Kabanov, "Relationship between Pluronic Block Copolymer Structure, Critical Micellization Concentration and Partitioning Coefficients of Low Molecular Mass Solutes," *Macromolecules*, vol. 33, no. 9, pp. 3305–3313, May 2000.

[20] G. K. Sarma, S. SenGupta, and K. G. Bhattacharyya, "Methylene Blue Adsorption on Natural and Modified Clays," *Sep. Sci. Technol.*, vol. 46, no. 10, pp. 1602–1614, 2011.

[21] G. Frens, "Controlled Nucleation for the Regulation of the Particle Size in Monodisperse Gold Suspensions," *Nature*, vol. 241, no. 105, pp. 20–22, Jan. 1973.

[22] R. J. Green, M. C. Davies, C. J. Roberts, and S. J. B. Tendler, "A surface plasmon resonance study of albumin adsorption to PEO–PPO–PEO triblock copolymers," *J. Biomed. Mater. Res.*, vol. 42, no. 2, pp. 165–171, 1998.

Acknowledgement:

This work was supported by the Sectoral Operational Programme for Human Resources Development 2007-2013, co-financed by the European Social Fund, under the project number POSDRU/107/1.5/S/76841 with the title „Modern Doctoral Studies: Internationalization and Interdisciplinarity".

LIST OF PUBLICATIONS

Papers published in ISI Journals:

1) **T. Simon**, S. Boca-Farcau, A.M. Gabudean, P. Baldeck, S. Astilean, *LED-activated methylene blue-loaded Pluronic-nanogold hybrids for in vitro photodynamic therapy,* **J. Biophotonics**, 1-10 **(2013)** doi:10.1002/jbio.201300058, (IF=3.099, IS=0.993);

2) **T. Simon**, S. Boca, D. Biro, P. Baldeck, S. Astilean, *Gold–Pluronic core–shell nanoparticles: synthesis, characterization and biological evaluation*, **J. Nanopart. Res.** 15 **(2013)** 1578. (IF= 2.175, FRI=0.673);

3) **T. Simon**, S. Boca, S. Astilean, *Pluronic-Nanogold hybrids: Synthesis and tagging with photosensitizing molecules*, **Colloids Surf. B** 97 **(2012)** 77-83. (IF= 3.554, IS=0.772);

4) M. Iliut, A.M. Gabudean, C. Leordean, **T. Simon**, C.-M. Teodorescu , S. Astilean, *Riboflavin enhanced fluorescence of highly reduced graphene oxide***, Chem. Phys. Lett**. (**2013),** manuscris acceptat (IF=2.145, IS=0.687);

5) B. Marta, E. Jakab, M. Potara, **T. Simon**, F. Imre-Lucaci, L. Barbu-Tudoran, O. Popescu, S. Astilean, *Pluronic-coated silver nanoprisms: synthesis, characterization and their antibacterial activity*, **Colloids Surf. A (2013**), doi:10.1016/j.colsurfa.2013.08.076, (IF=2.108, IS=0.585);

6) T. Gallavardin, M. Maurin, S. Marotte, **T. Simon**, A. M. Gabudean, Y. Bretonnière, M. Lindgren, F. Lerouge, P. L. Baldeck, O. Stéphan, Y. Leverrier, J. Marvel, S. Parola, O. Maury and C. Andraud, *Photodynamic therapy and two-photon bio-imaging applications of hydrophobic chromophores through amphiphilic polymer delivery*, **Photochem. Photobiol. Sci.** 10 **(2011)** 1216-1225. (IF= 2.584, IS=0.746).

Papers published in non ISI Journals:

1) Z. Benyey, E. Vanea, **T. Simon**, S. Cavalu, V. Simon, *Tetracycline loading and release from bioactive glass microspheres, STUDIA UBB PHYSICA, LVI, 2, 2011*